



HAL
open science

Phase and fluorescence imaging with a surprisingly simple microscope based on chromatic aberration

Ondřej Mandula, Jean-Philippe Kleman, Françoise Lacroix, Cédric Allier, Daniel Fiole, Lionel Hervé, Pierre Blandin, Dorothee Kraemer, Sophie Morales

► **To cite this version:**

Ondřej Mandula, Jean-Philippe Kleman, Françoise Lacroix, Cédric Allier, Daniel Fiole, et al.. Phase and fluorescence imaging with a surprisingly simple microscope based on chromatic aberration. *Optics Express*, 2020, 28 (2), pp.2079. 10.1364/OE.28.002079 . hal-02443413

HAL Id: hal-02443413

<https://hal.univ-grenoble-alpes.fr/hal-02443413v1>

Submitted on 27 Sep 2024

HAL is a multi-disciplinary open access archive for the deposit and dissemination of scientific research documents, whether they are published or not. The documents may come from teaching and research institutions in France or abroad, or from public or private research centers.

L'archive ouverte pluridisciplinaire **HAL**, est destinée au dépôt et à la diffusion de documents scientifiques de niveau recherche, publiés ou non, émanant des établissements d'enseignement et de recherche français ou étrangers, des laboratoires publics ou privés.



Distributed under a Creative Commons Attribution 4.0 International License



Phase and fluorescence imaging with a surprisingly simple microscope based on chromatic aberration

ONDŘEJ MANDULA,^{1,*} JEAN-PHILIPPE KLEMAN,²  FRANÇOISE LACROIX,² CEDRIC ALLIER,¹ DANIEL FIOLE,¹ LIONEL HERVÉ,¹ PIERRE BLANDIN,¹ DOROTHEE C. KRAEMER,¹ AND SOPHIE MORALES¹

¹Université Grenoble Alpes, CEA, LETI, DTBS, F-38000 Grenoble, France

²Université Grenoble Alpes, CEA, CNRS, IBS, F-38000 Grenoble, France

*ondrej.mandula@cea.fr

Abstract: We propose a simple and compact microscope combining phase imaging with multi-color fluorescence using a standard bright-field objective. The phase image of the sample is reconstructed from a single, approximately 100 μm *out-of-focus* image taken under semi-coherent illumination, while fluorescence is recorded *in-focus* in epi-fluorescence geometry. The reproducible changes of the focus are achieved with specifically introduced chromatic aberration in the imaging system. This allows us to move the focal plane simply by changing the imaging wavelength. No mechanical movement of neither sample nor objective or any other part of the setup is therefore required to alternate between the imaging modality. Due to its small size and the absence of motorized components the microscope can easily be used inside a standard biological incubator and allows long-term imaging of cell culture in physiological conditions. A field-of-view of 1.2 mm² allows simultaneous observation of thousands of cells with micro-meter spatial resolution in phase and multi-channel fluorescence mode. In this manuscript we characterize the system and show a time-lapse of cell culture in phase and multi-channel fluorescence recorded inside an incubator. We believe that the small dimensions, easy usage and low cost of the system make it a useful tool for biological research.

© 2020 Optical Society of America under the terms of the [OSA Open Access Publishing Agreement](#)

1. Introduction

Simple and compact microscopes present a significant advantage in biological research: compactness allows the system to be used directly in a standard incubator, while simplicity makes the microscope stable and robust.

Phase contrast and fluorescence microscopy are of particular interest in biomedical research. Phase imaging is a minimally invasive technique for the observation of non-absorbing, unstained specimens. The contrast in phase images reveals local changes of a sample's optical properties and allows observation of morphological changes. On the other hand, fluorescence can be used for highlighting specific structures, events or cell sub-populations. In other words, the phase-contrast image provides an overall context while fluorescence gives specificity.

A combination of these two complementary techniques is routinely implemented in classical phase-contrast, digital holography microscopy and other phase imaging setups [1–8], including commercially available systems. However, these microscopes are often bulky, in which case the long term observation of cell cultures is performed with an incubator built around the microscope increasing the size, complexity and cost of the instrument. Several compact non-commercial [9,10] and commercial systems [11,12] for fluorescence and phase imaging have been developed recently. It remains, however, challenging to combine high imaging performance with robustness and simplicity of the system.

Here we introduce a simple, non expensive and compact microscope ($10 \times 10 \times 30 \text{ cm}^3$) designed for phase and fluorescence imaging of cell cultures and other transparent samples directly in a standard incubator. Exploiting the chromatic aberration of a low-cost bright-field objective and using standard optomechanical pieces, we built a system, which does not require any mechanical movement of any setup components when changing between the phase and fluorescence modality. Additionally, the physical stability of the system reduces the sample drift and simplifies long-term observation of cell cultures. We propose our simple system as an original alternative to the existing methods.

2. Phase from defocus

Biologists have been observing phase samples with standard wide-field microscopes in slight defocus well before Zernike's invention of the phase-contrast technique [13]. Indeed, as shown in Fig. 1(a), bringing the sample out-of-focus creates contrasted fringes in the image plane and makes the transparent sample visible [14–16]. The obvious disadvantage of this method is a degradation of the image quality due to the blurring effect of defocus. However, under certain conditions, we can recover the phase and amplitude in-focus by numerical reconstructions.

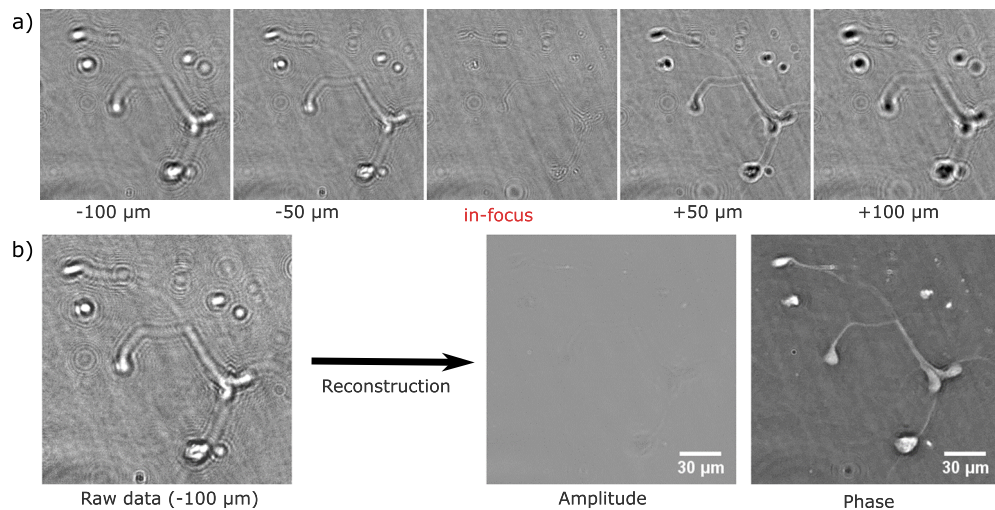


Fig. 1. (a) A demonstration of a non-absorbing (phase) sample (3 DIV hippocampal neurons) at different levels of defocus. The cells are almost invisible when brought in-focus (middle). (b) Our reconstruction of the in-focus phase-contrast image from a single, $100 \mu\text{m}$ defocused image taken under semi-coherent illumination.

Several techniques for reconstruction of defocused data have been developed. A method based on transfer of intensity equation (TIE) [17–21] has become popular, but it requires several images of the specimen taken at different degrees of defocus. Moreover, TIE is a valid approximation for small propagation distances, but the intensity contrast in the defocused image increases with propagation distance [22]. Larger defocus therefore facilitates the data acquisition and increases the sensitivity of the technique. A reconstruction of a set of images with larger defocus distances has been proposed in [23,24]. Paganin filter [25] estimating phase and intensity of a weakly refracting object from a single defocused image is currently used in x-ray imaging. However, the method is approximating only the first fringe of the Fresnel diffraction pattern, which in our settings significantly limits the recovery of high spatial frequencies and therefore reduces the resolution of the reconstructed images.

In this manuscript we use a reconstruction of a single, approximately $100\ \mu\text{m}$ defocused image [26] as shown in Fig. 1(b). This reconstruction algorithm is based on an iterative, constrained optimization of the Fresnel diffraction model for coherent light [27,28] and is described in more details in Sec. 7.

3. Combining phase imaging with fluorescence using chromatic aberration

A combination of our phase imaging method with fluorescence requires the sample to be out-of-focus for phase imaging, while it must be in-focus for fluorescence imaging, as the incoherent nature of fluorescence does not allow back-propagation of the defocused fluorescence image. Moreover, the signal-to-noise ratio of fluorescence drops dramatically with an increasing extent of defocus.

Here, we propose a system, which allows to record the fluorescence images in-focus and brings the sample out-of-focus for phase imaging without mechanical movement of neither the sample nor the objective, simplifying both the system and the data acquisition procedure. The changes of the focal plane are achieved with chromatic aberration of a Motic EC Plan $10\times/0.25\text{NA}$ objective combined with a short focal length ($f = 50\ \text{mm}$) tube-lens. This produces a displacement of the focal plane as shown in Fig. 2(a). Note that this system (objective + tube-lens) is achromatic within the theoretical depth of field ($\sim 10\ \mu\text{m}$, red band in Fig. 2(a)), in the range $500\ \text{nm} - 600\ \text{nm}$, while it is strongly chromatic for shorter wavelengths (Fig. 2(a)). For example, we can achieve $100\ \mu\text{m}$ defocus by changing the light from $500\ \text{nm}$ to $420\ \text{nm}$. This allows us to move the focal plane simply by changing the imaging wavelength as shown in Fig. 3. With our chromatic system, we can keep the green and red fluorescent signals in-focus (Figs. 3(a,d) and 3(b,e)) and use illumination with $\lambda = 420\ \text{nm}$ to bring the sample $100\ \mu\text{m}$ out-of-focus (Figs. 3(c,f)). To record multi-colour fluorescence we used a single multi-band fluorescence filter set (see Fig. 2(b) and Sec. 4). Note, that when placed in-focus for green fluorescence, the red emission ($580 - 650\ \text{nm}$) is partially outside the depth-of-field of the objective ($5\ \mu\text{m}$ defocus at $580\ \text{nm}$ and $20\ \mu\text{m}$ defocus at $650\ \text{nm}$ with respect to green fluorescence at $520\ \text{nm}$, see Fig. 2(a)), which limits the quality of the red-fluorescence image. The defocused image at $420\ \text{nm}$ passes through the blue emission band of the filter set (black curve in Fig. 2(b)).

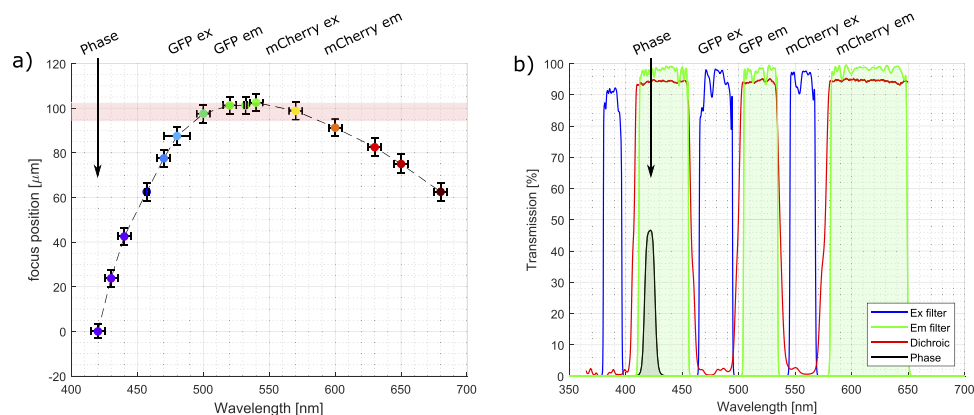


Fig. 2. a) Measured chromatic displacement of the focus. The theoretical depth of field of the system ($10\ \mu\text{m}$) is shown as a red band. While the system is approximately achromatic in the range $\lambda = 500 - 600\ \text{nm}$ (green to red), it is strongly chromatic at $\lambda = 420\ \text{nm}$ (violet). b) Multi-band fluorescent filter set with a phase (defocus) imaging filter at $\lambda = 420\ \text{nm}$ passing through the blue emission band.

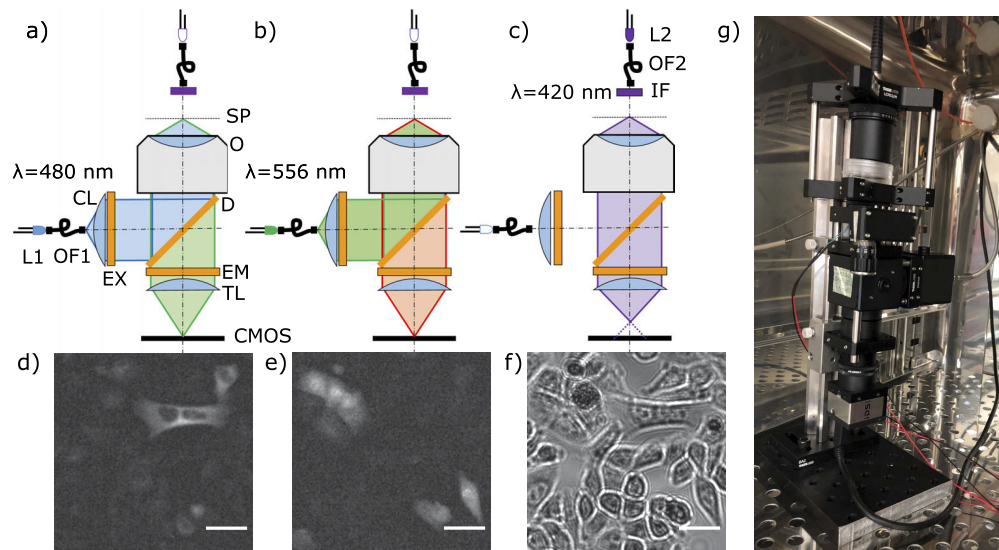


Fig. 3. System in fluorescence (a-b) and phase (c) mode. Note the defocus due to chromatic aberration in (c). L1 blue and green LEDs for fluorescence excitation, L2 blue LED for defocused imaging in transmission mode with a narrow band filter IF. OF optical fibre, CL collimator lens, EX excitation filter, D dichroic, EM emission filter, O objective, SP sample plane, CMOS camera. (d,e) Regions of interests (ROIs) of in-focus green and red fluorescence, respectively. (f) Corresponding ROI of raw out-of-focus data. Scale bar $50\ \mu\text{m}$. (g) The system installed in an incubator.

Note that chromatic aberration has been previously proposed for other applications. For example, encoding the axial position in optical profilometers [29] and in chromatic confocal microscopes [30]. Small focal changes ($\sim 1\ \mu\text{m}$) due to chromatic aberration have been used to solve the transport of intensity equation and recover the phase image [21].

4. Setup

Standard Thorlabs components are used for housing of the optics and the camera. The setup is designed to reduce the vibration, sample drift and long term focal drift (see Fig. 3(g)). Image acquisition and illumination are controlled with a Raspberry Pi [31]. The image reconstruction is performed on a separate computer (see Sec. 7).

Fluorescence is recorded in epi-fluorescence configuration, whereas phase (defocus) imaging is recorded in transmission geometry as shown in Fig. 3(a), 3(b) and 3(c), respectively. The excitation source of the fluorescence modality, the blue and green LEDs L1, (Cree LED, max 450 nm, FWHM 18 nm, max 539 nm, FWHM 34 nm) are coupled with a $1500\ \mu\text{m}$ diameter multi-mode optical fibre OF1 (Thorlabs M107L01) and are collimated with a fibre collimator CL (Thorlabs F220SMA-532). Light passes through the excitation filter EX, which is a part of the multi-band fluorescence filter set (Semrock DA/FI/TR-A-000, see Fig. 2(b)). Afterwards the light is reflected by a dichroic D towards the sample SP through the objective O (Objective $10\times/0.25\text{NA}$ Motic EC Plan). The fluorescence signal is collected by the same objective O and then passes through the dichroic D and the multi-band emission filter EM. The in-focus image, created by a tube-lens TL ($f = 50\ \text{mm}$, Thorlabs AC254-050-A), is registered with an industrial monochrome camera CMOS (IDS UI-1480SE, $2.2\ \mu\text{m}$ pixel-size, 2560×1920 pixels, 8 bits), as shown in Fig. 3(d) and 3(e).

Our filter set allows adding an additional excitation LED (Thorlabs, LED375L) in the spectral band 380 – 397 nm (Fig. 2(b)). This broadens the applicability to the nuclear stain Hoechst 33342 (ThermoFisher). The peak of Hoechst 33342 emission is at 453 nm, where the system is strongly chromatic (see Fig. 2(a)) and the blue fluorescence signal is therefore out-of-focus. However, the broad emission spectrum of Hoechst 33342 allows detection in the green fluorescence band of the filter set, see Fig. 4 showing triple stained HeLa cells with Hoechst, GFP and mCherry.

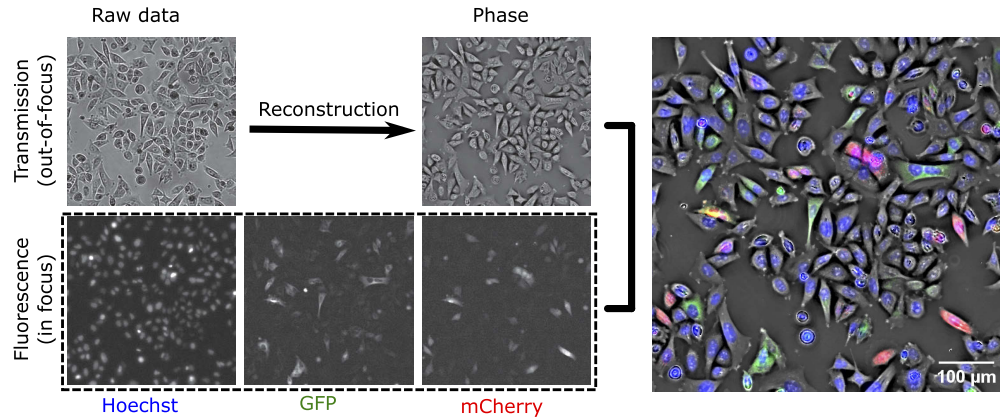


Fig. 4. ROI of a snapshot from 40h recording of triple stained HeLa cell culture (Blue - Hoechst staining cell nucleus, Green - GFP tubulin, Red - mCherry). Raw defocused images taken in transmission mode are numerically reconstructed to yield an in-focus phase-contrast image of the sample. This can be combined with the corresponding in-focus epi-fluorescence data (dashed box) producing a phase (gray) and fluorescence (RGB) combined image (right).

The phase (defocus) imaging modality is depicted in Fig. 3(c). Blue LED **L2** (CREE, max 450 nm, FWHM 18 nm) is coupled with a multi-mode, 400 μm diameter optical fibre **OF2** (Thorlabs M45L01), which passes through a narrow band illumination filter **IF** (420 nm, FWHM 10 nm, Thorlabs FB420-10). The light passes through the sample which is located at 5 cm distance from the exit of the fibre. The transmitted light is collected with the objective **O** and then passes through the blue emission band of the filter set (Fig. 2(b)). Due to the chromatic aberration the image recorded on the **CMOS** camera is $\sim 100 \mu\text{m}$ out-of-focus (see Fig. 3(f)).

We can make a simple estimation of the coherence properties of the illumination source from the geometry of the setup. The spatial coherence length of the illumination source for phase imaging can be estimated to $l_s \approx d\lambda/D \approx 50 \mu\text{m}$, with λ being the wavelength of the illumination source, d the distance between the exit of the fibre and the sample and D the diameter of the fibre. The temporal coherence length is estimated to $l_t \approx \lambda^2/\Delta\lambda \approx 18 \mu\text{m}$, with $\Delta\lambda$ being the spectral width of the source.

The power measured at the sample plane was 3.4 μW for defocus imaging ($\lambda = 420 \text{ nm}$), 0.15 mW for UV excitation ($\lambda = 375 \text{ nm}$), 0.5 mW for blue excitation ($\lambda = 488 \text{ nm}$) and 0.38 mW for green excitation ($\lambda = 560 \text{ nm}$). The diameter of the fluorescence excitation beam (FWHM of the gaussian profile) was approximately 3 mm.

Note that the focal length of a standard tube-lens of a 10 \times /0.25NA Motic objective is 180 mm. Using a short tube-lens ($f = 50 \text{ mm}$) results in a 2.8 \times magnification with a field-of-view (FOV) of 3 mm².

To measure the chromaticity of our system (Fig. 2(a)), we used a set of different band pass filters covering the range 420 nm - 680 nm. For each filter we determined the focal position of a sample plotted in Fig. 2(a). The FWHM of the spectral band for each filter are plotted as the

horizontal error bars. The vertical error bars were estimated from repeated measurements and set to 5 μm for all measured points.

5. Sample preparation

Polyclonal HeLa cells expressing variable amounts of EGFP-tubulin (see [32] for details) were plated at 50% density in a 35 mm glass-bottom petri dish (Ibidi) in Dulbecco's Modified Eagle's Medium (DMEM, Gibco) supplemented with 10% foetal bovine serum (Hyclone). One day after plating, cells were transfected with pmCherry-N1 (Clontech) using jetPRIME (Polyplus, transfection efficiency above 50%), resulting in a mixed population of unstained, green and red cells, as well as a subpopulation of cells expressing both fluorescent proteins. Prior to microscopy, the transfection medium is replaced with fresh medium supplemented with 2.5 $\mu\text{g/ml}$ Hoechst 33342 (Sigma-Aldrich) for nuclei counter-staining. After 10 minutes at 37°C, the medium is replaced by 2 ml of phenol red-free complete DMEM/F-12 (Gibco) containing 15 mM HEPES for imaging.

SYTO9 (ThermoFisher) in a final concentration 100 nM was used for staining *Micrococcus luteus* bacteria. After 5 min of incubation, the solution was mixed with a suspension of 2 μm polystyrene beads (Fluka Analytical) and inserted into 100 μm thick Countess Cell Counting Chamber Slides (ThermoFisher) for observation.

6. Data acquisition

We installed the system directly in a standard biological incubator (see Fig. 3(g)). A glass bottom Petri dish (glass-bottom 35 mm dishes, Ibidi), containing the sample, was placed on a rigid platform above the objective. The time-lapse acquisition can be started after manually bringing the objective to the focus position of green or red fluorescence signal. The exposure time for defocus data was 70 ms (0% gain). The exposure time for fluorescence data was 500 ms (50% gain) for Hoechst 33342, 1000 ms (50% gain) for GFP, 1000 ms (50% gain) for mCherry and 340 ms (0% gain) for SYTO9. The green fluorescence, red fluorescence and defocused images were taken sequentially with approximately 5 s delay caused by transfer of the images from the camera to the computer.

7. Data reconstruction and image processing

The recorded out-of-focus raw data are passed on to a reconstruction procedure. Our reconstruction algorithm is based on an iterative optimization of the Fresnel diffraction model for coherent light [27] under the assumption of a weak perturbation of the incident field ([16,33]). The field at a distance z from the sample is described by the convolution

$$A_z(\mathbf{r}) = A_0(\mathbf{r}) * h_z(\mathbf{r}), \quad (1)$$

where $A_0(\mathbf{r})$ is the optical field at the sample plane and \mathbf{r} are the spatial coordinates. h_z is the Fresnel propagator

$$h_z(\mathbf{r}) = \frac{1}{i\lambda z} \exp\left(\frac{i\pi\mathbf{r}^2}{\lambda z}\right). \quad (2)$$

The reconstruction process optimizes the optical field at the sample plane $A_0(\mathbf{r}) = |A_0(\mathbf{r})|e^{i\phi(\mathbf{r})}$, while maintaining perfect agreement with the intensity measurement at the sensor plane $I_z = |A_z|^2$. The reconstruction contains regularization terms based on total variation constraints as described in [28] and soft constraints on absorbance of the reconstructed sample. The term to be minimised

is described by

$$\epsilon(A_0) = c_1 \int_{\mathbb{R}^2} d\mathbf{r} |\nabla A_0(\mathbf{r})| + c_2 \int_{\Omega} d\mathbf{r} |A_0(\mathbf{r})|^2, \quad (3)$$

with Ω being the region, where $|A_0| > \sqrt{I_z}$. For the reconstruction presented in this manuscript we chose $c_1 = 1$ and $c_2 = 10$ guided by visual inspection of the reconstructed images. A parameter choice based on Bayesian inference has been proposed in [24].

In the current algorithm the partial coherence of the illumination is not taken into account. The out-of-focus distance can be determined from the reconstruction performed at different axial positions z . To determine the focused image, an auto-focus algorithm or a manual selection can be employed. In the time-lapse acquisition the defocus is determined from the final image and subsequently used for the reconstruction of the whole sequence.

The reconstruction of a single 10 Mpixel image lasts approximately 3 minutes on our standard desktop computer (Processor Intel(R) Xenon(R) CPU E3-1240 v5 @ 3.50GHz with 32GB RAM and NVIDIA Quadro K2200 graphic card).

Reconstructed phase-contrast image in gray is combined with false colored fluorescence images, despeckled with a 3×3 pixels median filter and background subtracted with 'rolling ball' algorithm ($r = 50$ pixels) [34] using ImageJ plugins [35] to create a composite image shown in Fig. 4.

8. Results

The resolution of the system was determined from the in-focus images of the absorption USAF resolution target as shown in Fig. 5. We can resolve (with 20% contrast) down to the 5th element

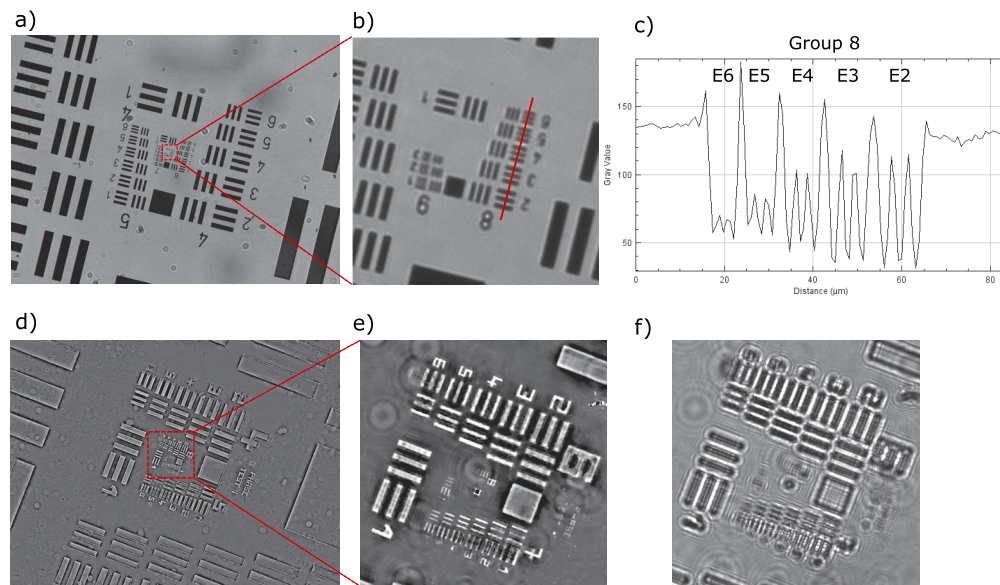


Fig. 5. USAF absorption (a-c) and phase (d-f) resolution target imaged with our system. a) Full field-of-view of absorption resolution target imaged in-focus, b) central ROI (red box in a)). We can resolve group 8, element 5 with line width of $1.23 \mu\text{m}$. c) line profile over group 8 (red line in b)). d) Reconstructed phase image of phase resolution target (silica slide with 300 nm thick engraving of the USAF resolution target) taken at $100 \mu\text{m}$ defocus. e) Central region (red box in d)) showing groups 6, 7 and 8. f) $100 \mu\text{m}$ defocused image (raw data) of a region shown in e).

of group 8 with $1.23\ \mu\text{m}$ line width (Fig. 5(b) and 5(c)). The spatial resolution can be estimated as twice this distance to $2.46\ \mu\text{m}$ (the line-pair distance). The reconstruction of a $100\ \mu\text{m}$ defocused image (Fig. 5(f)) of our custom-made phase resolution target (silica slide with $300\ \text{nm}$ thick engraving of the USAF resolution target) in Fig. 5(d) and 5(e) shows that at least the 2nd element of group 8 (line width $1.74\ \mu\text{m}$, line-pair distance $3.48\ \mu\text{m}$) can be resolved. Unfortunately smaller elements of our phase resolution target were not properly engraved as checked with a high NA objective on a different phase-contrast microscope (data not shown). As a result we could not establish the resolution limit of the phase-contrast modality of our system.

We used our microscope for the observation of HeLa cell culture marked with Hoechst 33342 and a sub-population of cells expressing GFP tubulin or mCherry (see Sec. 5). Fluorescence and defocus images were recorded every 10 min over 40 hours directly in the incubator. The full FOV ($\sim 3\ \text{mm}^2$) is shown in Fig. 6. Note that the quality of the image decreases at the periphery of the image Fig. 6. As discussed in Sec. 4 the short focal length tube-lens results in a larger FOV, however, is decreases the image quality. We can expect that the flat-field correction of the objective is effective only over a central part of the FOV. The region with optimal image quality, where the flat field correction is better than the theoretical depth-of-field ($10\ \mu\text{m}$) is encircled in Fig. 6, resulting in a $1.2\ \text{mm}^2$ FOV containing ~ 700 cells at $t = 20$ hours.

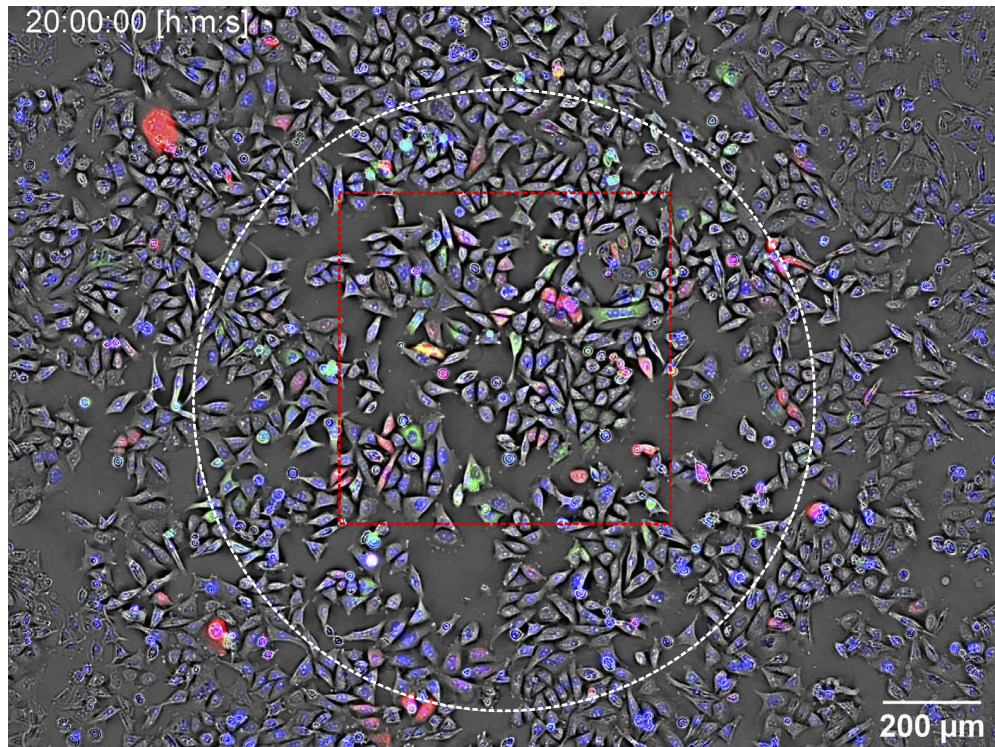


Fig. 6. HeLa cells culture in combined phase contrast (gray) and fluorescence image. Hoechst stain marking cell nucleus is shown in blue, eGFP marking α -tubulin structures in green and non-specific pmCherry in red. Whole field of view ($3\ \text{mm}^2$) with circular region ($1.2\ \text{mm}^2$) with acceptable flat field correction (white circle). There is ~ 700 cells contained in the circular region. ROI shown with red dashed box at 5-hour intervals is shown in Fig. 7(a).

Snapshots of the central region of interest (ROI) in 5-hour intervals are shown in Fig. 7(a). The cells were dividing up to confluence at $t = 40$ hours. For time-lapse movie see Visualization 1. The phase images Fig. 7(b) show details of the individual cells. Nucleus with nucleoli and details

of thin and dynamic lamellipodia can be observed. Red arrows point to the cells in division. Due to the large optical thickness of the mitotic cells the algorithm encounters phase-wrapping problems. Phase unwrapping will be addressed in future work.

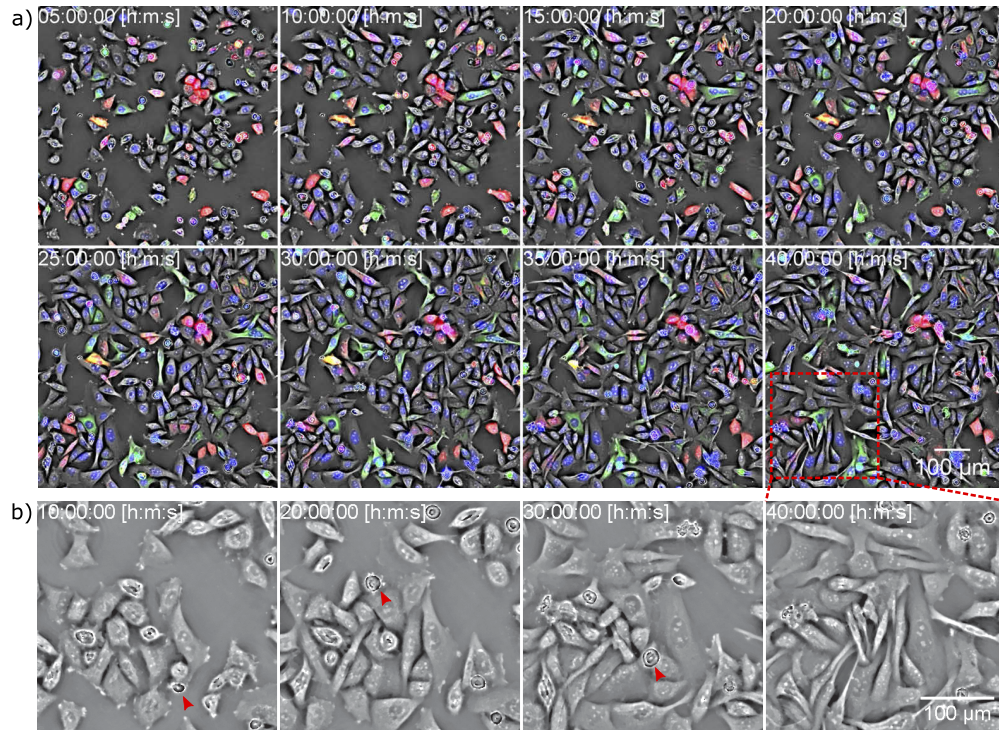


Fig. 7. Time-lapse of triple stained HeLa cells. Images taken every 10 mins over 40 hours.

a) Selected ROI from Fig. 6 shown at 5-hour intervals (see also Visualization 1). b) A small ROI of reconstructed phase image. Cells in division show phase wrapping (red arrows).

To further explore the resolution limits of our system, we acquired phase and fluorescence images of $2\ \mu\text{m}$ polystyrene beads (non fluorescent) mixed with *Micrococcus luteus* marked with SYTO9 Green Fluorescent Nucleic Acid Stain. Figure 8(a) shows the combined phase and fluorescence image with three enlarged regions showing bacteria and beads. Figure 8(b) is the enlarged reconstructed phase-contrast image of the red box in Fig. 8(a). We can observe both the bacteria (several are pointed out with arrows) and the individual beads (two beads are pointed out with boxes). The distinction between the beads and the bacteria can easily be made based on the corresponding fluorescence image Fig. 8(c). The multimer structure of the cocci clusters, dimers, tetramers and irregular multimers, can be barely resolved in the fluorescence image. The size of a single coccus is $0.5 - 1\ \mu\text{m}$, which is at the estimated resolution limit of the instrument (see Fig. 5). The multimer structures are less resolved in the phase contrast image Fig. 8(b). Note that we used a $100\ \mu\text{m}$ thick chamber (see Sec. 5). The beads were distributed throughout the volume with certain sedimenting at the bottom. The bacteria were mostly deposited at the bottom of the chamber. The reconstruction was performed at the plane of focus of the bacteria and therefore some beads are out-of-focus with distinct fringes (see red box in Fig. 8(b)). A detailed inspection of a composite image (inset in Fig. 8(a)) shows that there is a slight local displacement between the phase and fluorescence image due to Brownian motion and the few seconds delay between the capture of the defocused and fluorescence image (see Sec. 6). Chromatic aberration also results in slightly different magnification for phase and fluorescence images, noticeable at the periphery.

The distortion of the point-spread function at the periphery of the image is also apparent in the insets of Fig. 8(a).

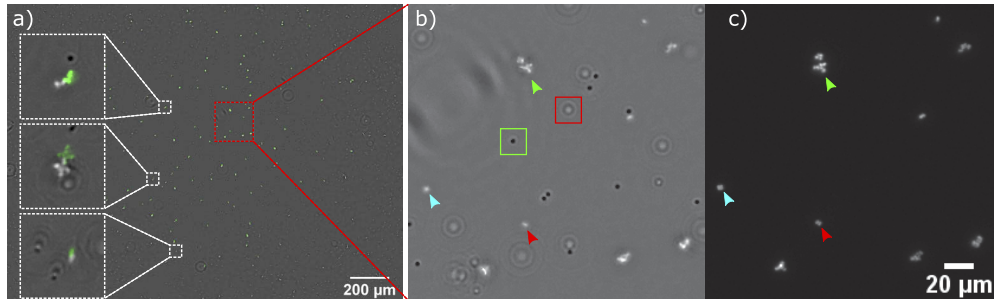


Fig. 8. a) Phase contrast image (gray) with overlaid fluorescence (green) of *Micrococcus luteus* marked with SYTO9 in mixture with $2\ \mu\text{m}$ polystyrene beads. Insets show the local displacement between phase and fluorescence image. Reconstructed phase contrast image of ROI marked with red box is shown in b), corresponding fluorescence image is shown in c) with arrows highlighting several *Micrococcus* clusters. The structure of the clusters, the dimers (red), tetramers (cyan) and multimers (green) of cocci, is at the resolution limit of our system. Two beads above and at the focal plane are highlighted with a red and green box, respectively.

9. Discussion

Our phase and fluorescence system is remarkably simple and robust. We have not observed any noticeable focal or lateral drift during the experiments lasting several days. The changes of the focus caused by chromatic aberration are perfectly reproducible, further simplifying the time-lapse recordings. We were observing dividing cells even after 40 hours of recording with 10-min intervals (240 cycles of triple fluorescence and phase equals 960 recorded images in total) demonstrating the capabilities of our system to monitor the cells over several days in a minimally invasive manner.

However, there are limitations that should be discussed. The image quality is degraded at the periphery as can be seen in Fig. 6(a) and Fig. 8(a) and equally fluorescence detection deteriorates in the peripheral areas. This is a consequence of field curvature and spherical aberration that are introduced due to a combination of the low-cost (\$40) Motic EC Plan 10 \times /0.25NA objective and a short tube-lens ($f = 50\ \text{mm}$). This specific combination is however required to obtain the strong chromatic aberration in the range 400 nm – 500 nm with 100 μm shift of focus (Fig. 2(a)).

At present, we do not make claims about the quantitative nature of the reconstructed phase images and we cannot quantitatively determine the optical path difference introduced by the sample [36]. The phase should be taken as a qualitative visualization of transparent samples in the same manner as the Zernike's phase contrast or DIC images. Our phase-contrast images show the cellular morphologies, the cellular density, the kinetics and dynamics as well the overall context of the experiment.

The important aspect of the quantitative nature of the phase images is currently addressed by us through the development of a new reconstruction procedure, combining our propagation-based reconstruction with methods inspired by TIE [21] and with recordings at different defocus [24,37]. For example, recording at 420 nm, 430 nm and 440 nm results in, respectively, 100 μm , 75 μm and 55 μm defocus compared to the green fluorescence signal at 500 nm (see Fig. 2(a)). The unwrapping problem and the partial coherence of the source should also be taken into account.

In summary, we are taking advantage of the imperfection of our imaging system to create an inexpensive, compact and robust phase and multi-channel fluorescence microscope. We

believe that the simplicity and robustness of the system together with its minimal cost and space requirements are highly beneficial to the bio-imaging community.

Acknowledgement

We acknowledge the financial support of the Cross-Disciplinary Program on Instrumentation and Detection of CEA, the French Alternative Energies and Atomic Energy Commission.

Disclosures

O. Mandula and C. Allier are inventors of a patent devoted to the chromatic system for phase and fluorescence imaging.

References

1. F. Zernike, "Phase contrast, a new method for the microscopic observation of transparent objects," *Physica* **9**(7), 686–698 (1942).
2. G. Nomarski, "Differential microinterferometer with polarized waves," *J. Phys. Radium* **16**, 9S–11S (1955).
3. M. K. Kim, *Digital Holographic Microscopy* (Springer, 2011).
4. W. Osten, A. Faridian, P. Gao, K. Körner, D. Naik, G. Pedrini, A. Kumar Singh, M. Takeda, and M. Wilke, "Recent advances in digital holography," *Appl. Opt.* **53**(27), G44–63 (2014).
5. Y. Park, G. Popescu, K. Badizadegan, R. R. Dasari, and M. S. Feld, "Diffraction phase and fluorescence microscopy," *Opt. Express* **14**(18), 8263 (2006).
6. X. Quan, K. Nitta, O. Matoba, P. Xia, and Y. Awatsuji, "Phase and fluorescence imaging by combination of digital holographic microscopy and fluorescence microscopy," *Opt. Rev.* **22**(2), 349–353 (2015).
7. I. de Kernier, A. Ali-Cherif, N. Rongeat, O. Cioni, S. Morales, and J. Savatier, "Large field-of-view phase and fluorescence mesoscope with microscopic resolution," *J. Biomed. Opt.* **24**(03), 1–9 (2019).
8. <http://phasicscorp.com/sectors/life-science>.
9. K. Sasagawa, A. Kimura, M. Haruta, T. Noda, T. Tokuda, and J. Ohta, "Highly sensitive lens-free fluorescence imaging device enabled by a complementary combination of interference and absorption filters," *Biomed. Opt. Express* **9**(9), 4329–4344 (2018).
10. Q. Lu, G. Liu, C. Xiao, C. Hu, S. Zhang, R. X. Xu, K. Chu, Q. Xu, and Z. J. Smith, "A modular, open-source, slide-scanning microscope for diagnostic applications in resource-constrained settings," *PLoS One* **13**(3), e0194063 (2018).
11. <https://www.essenbioscience.com/en/products/incucyte>.
12. <https://www.thermofisher.com/order/catalog/product/AMF7000>.
13. F. Zernike, "How I Discovered Phase Contrast," *Science* **121**(3141), 345–349 (1955).
14. U. Agero, C. H. Monken, C. Ropert, R. T. Gazzinelli, and O. N. Mesquita, "Cell surface fluctuations studied with defocusing microscopy," *Phys. Rev. E* **67**(5), 051904 (2003).
15. U. Agero, L. Mesquita, B. Neves, R. Gazzinelli, and O. Mesquita, "Defocusing microscopy," *Microsc. Res. Tech.* **65**(3), 159–165 (2004).
16. C. J. R. Sheppard, "Defocused transfer function for a partially coherent microscope and application to phase retrieval," *J. Opt. Soc. Am. A* **21**(5), 828–831 (2004).
17. M. R. Teague, "Image formation in terms of the transport equation," *J. Opt. Soc. Am. A* **2**(11), 2019–2026 (1985).
18. N. Streibl, "Phase imaging by the transport equation of intensity," *Opt. Commun.* **49**(1), 6–10 (1984).
19. W. Yu, X. Tian, X. He, X. Song, L. Xue, C. Liu, and S. Wang, "Real time quantitative phase microscopy based on single-shot transport of intensity equation (sstie) method," *Appl. Phys. Lett.* **109**(7), 071112 (2016).
20. C. Zuo, Q. Chen, W. Qu, and A. Asundi, "High-speed transport-of-intensity phase microscopy with an electrically tunable lens," *Opt. Express* **21**(20), 24060 (2013).
21. L. Waller, S. S. Kou, C. J. Sheppard, and G. Barbastathis, "Phase from chromatic aberrations," *Opt. Express* **18**(22), 22817–22825 (2010).
22. R. Hofmann, J. Moosmann, and T. Baumbach, "Criticality in single-distance phase retrieval," *Opt. Express* **19**(27), 25881 (2011).
23. P. Cloetens, W. Ludwig, J. Baruchel, D. Van Dyck, J. Van Landuyt, J. P. Guigay, and M. Schlenker, "Holotomography: Quantitative phase tomography with micrometer resolution using hard synchrotron radiation x rays," *Appl. Phys. Lett.* **75**(19), 2912–2914 (1999).
24. F. Fus, Y. Yang, A. Pacureanu, S. Bohic, and P. Cloetens, "Unsupervised solution for in-line holography phase retrieval using Bayesian inference," *Opt. Express* **26**(25), 32847 (2018).
25. D. Paganin, S. C. Mayo, T. E. Gureyev, P. R. Miller, and S. W. Wilkins, "Simultaneous phase and amplitude extraction from a single defocused image of a homogeneous object," *J. Microsc.* **206**(1), 33–40 (2002).
26. O. Mandula, C. Allier, L. Hervé, E. Denarier, A. Fourest-Lieuvain, S. Gory-Fauré, A. Vinit, and S. Morales, "Phase from defocus," in *Quantitative Phase Imaging IV*, vol. 10503 G. Popescu and Y. Park, eds., International Society for Optics and Photonics (SPIE, 2018), pp. 112–123.

27. J. W. Goodman, *Introduction to Fourier optics* (Roberts and Company Publishers, 2005).
28. L. Herve, O. Cioni, P. Blandin, F. Navarro, M. Menneteau, T. Bordy, S. Morales, and C. Allier, "Multispectral total-variation reconstruction applied to lens-free microscopy," in *Quantitative Phase Imaging IV*, vol. 10503 G. Popescu and Y. Park, eds., International Society for Optics and Photonics (OSA, 2018), pp. 5828–5836.
29. G. Molesini, G. Pedrini, P. Poggi, and F. Quercioli, "Focus-wavelength encoded optical profilometer," *Opt. Commun.* **49**(4), 229–233 (1984).
30. M. A. Browne, O. Akinyemi, and A. Boyde, "Confocal surface profiling utilizing chromatic aberration," *Scanning* **14**(3), 145–153 (1992).
31. <https://www.raspberrypi.org/>.
32. C. Mollinari, J.-P. Kleman, Y. Saoudi, S. A. Jablonski, J. Perard, T. J. Yen, and R. L. Margolis, "Ablation of PRC1 by small interfering RNA demonstrates that cytokinetic abscission requires a central spindle bundle in mammalian cells, whereas completion of furrowing does not," *Mol. Biol. Cell* **16**(3), 1043–1055 (2005).
33. M. Born and E. Wolf, *Principles of optics*, vol. 1 (Cambridge University Press, 1999).
34. S. Sternberg, "Biomedical image processing," *Computer* **16**(1), 22–34 (1983).
35. J. Schindelin, I. Arganda-Carreras, E. Frise, V. Kaynig, M. Longair, T. Pietzsch, S. Preibisch, C. Rueden, S. Saalfeld, B. Schmid, and J.Y. Tinevez, "Fiji: an open-source platform for biological-image analysis," *Nat. Methods* **9**(7), 676–682 (2012).
36. C. Allier, L. Hervé, O. Mandula, P. Blandin, Y. Usson, J. Savatier, S. Monneret, and S. Morales, "Quantitative phase imaging of adherent mammalian cells: a comparative study," *Biomed. Opt. Express* **10**(6), 2768–2783 (2019).
37. A. Greenbaum and A. Ozcan, "Maskless imaging of dense samples using pixel super-resolution based multi-height lensfree on-chip microscopy," *Opt. Express* **20**(3), 3129–3143 (2012).